IEEE Access
Multidisciplinary | Rapid Review | Open Access Journal

Received March 4, 2020, accepted March 23, 2020, date of publication March 26, 2020, date of current version April 13, 2020.

Digital Object Identifier 10.1109/ACCESS.2020.2983518

Design, Optimization and Energetic Evaluation of an Efficient Fully Powered Ankle-Foot Prosthesis With a Series Elastic Actuator

DIANBIAO DONG[1,2], WENJIE GE[1], BRYAN CONVENS[2], YUANXI SUN[3], TOM VERSTRATEN[2], AND BRAM VANDERBORGHT[2]

[1]School of Mechanical Engineering, Northwestern Polytechnical University, Xi'an 710072, China
[2]Department of Mechanical Engineering, Vrije Universiteit Brussel, 1050 Brussels, Belgium
[3]College of Mechanical Engineering, Chongqing University, Chongqing 400044, China

Corresponding author: Wenjie Ge (gwj@nwpu.edu.cn)

This work was supported in part by the National Natural Science Foundation of China under Grant 50975230, and in part by ERC under Grant 337596 SPEAR.

ABSTRACT The use of powered ankle-foot prostheses for below-knee amputees leads to challenges like the peak power of the applied actuator and biomechanical features of the prosthesis foot. This paper proposes an efficient powered ankle-foot prosthesis with a series elastic actuator. By combining the geared five-bar spring (GFBS) mechanism and the traditional series elastic actuator (SEA), a series elastic with geared five-bar (SGFB) actuator is built. The new SGFB actuator has the benefits of both the GFBS and the SEA on mimicking biomechanics of the human ankle and reducing the peak power of the motor. The healthy walking gait in the experiment results indicates that the optimized SGFB prosthesis foot including a 150W Maxon DC motor can provide a 70kg subject enough net positive energy with an energy efficiency of 35.3% during normal speed walking in the treadmill trials. The experiment of the SGFB prosthesis foot in semi-active mode shows the advantage on closely mimicking the human biomechanics during the control dorsiflexion phase and the importance of injecting positive energy during the powered plantarflexion phase. The experiment results also show that the optimization of different parameters within the electromechanical model considering the efficiency of the whole drive train can effectively reduce the motor's peak power to 132 W by making the motor more effective in high-power conditions.

INDEX TERMS Actuator, efficiency, peak power, prosthesis, series elastic actuator.

I. INTRODUCTION

Below-knee amputation is one of the major amputations due to increasing number of peripheral vascular diseases and traffic accidents [1]. Large number of ankle-foot prostheses are designed and produced to meet the desire of lower-limber amputees participating in the daily activities. These designs are often based on the kinetics and dynamics of the able-bodied human ankle, which have been recorded by several researchers using different methods [2]–[4]. Until now, most of ankle-foot prostheses in the current commercial market are still passive. According to the biomechanics of the human ankle, the most popular passive foot named energy store and return (ESAR) foot is designed to provide a resisting torque and store energy during the controlled dorsiflexion phase and return the stored energy during the following push-off phase. However, in contrast to the human ankle, researches show that the energy stored during control dorsiflexion phase in the ESAR foot is not enough for the following positive power phase. The passive foot cannot produce net positive energy itself. The insufficient energy features of passive ankle-foot prostheses may lead to the limitation of walking speed, rotation range, increased metabolic energy costs and nonsymmetrical walking gait. Hence, the additional active power is needed for the prosthetic foot to better mimic the dynamics of the human ankle. In past few years, more and more studies are focused on the design and validation of novel powered ankle-foot prostheses [5]–[14].

One of the primary issues in the area of the powered ankle-foot prosthesis is the high demand of the peak power for the actuator system [15], [16]. According to the human biomechanics, more than 250 W of mechanical power is needed for a 75 kg able-bodied person at normal walking speed. The high peak power gives a limitation to the size

The associate editor coordinating the review of this manuscript and approving it for publication was Aysegul Ucar.

and weight of the applied actuator system. To reduce the power requirement of the powered ankle-foot prostheses, the concept of the compliant actuator [17], [18] is widely implemented in the modeling and design of the powered ankle foot prosthesis. Hitt *et al.* [19], [20] proposed an active prosthetic foot composed of a series elastic actuator (SEA) [21]–[23]. Based on the SEA, the required power of the DC motor is effectively reduced to 150W. Herr and Grabowski [24] designed a bionic ankle-foot prosthesis with new actuator system including a 200W DC motor can 67% efficiently produce 20J of positive energy during the stance phase by combining a series-elastic actuator and a parallel unidirectional leaf spring (SEPA) for an 80 kg amputee walking at 0.75m/s to 1.75m/s. Gao *et al.* [25] proposed a novel powered ankle foot prosthesis composed of a novel nonlinear parallel spring mechanism. By using a typical parallel elastic actuator [27], [28], the peak power of the DC motor can be decreased by 37.5%. Convens *et al.* [26] proposed an active energy-efficient propulsive prosthesis foot integrated with a clutched SEA actuator. The specific clutch enables the prosthesis foot to adapt to terrains with different slope. By optimizing the parameters of the SEA actuator and utilizing the clutch, the energy consumption is reduced to 17.7J during normal speed level-ground walking. Hence, it has been proven that the concept of the compliant actuator can effectively reduce the power requirement of the active prosthetic foot by different combinations. Besides, considering the electrical efficiency model (EEM) [27], [28] of the DC motor and the gearbox, the electromechanical modeling [29] of the prosthesis's architecture and reasonable optimization of some parameters [15], [16], [30] can also provide a decrease in the mechanical and electrical power required by the motor.

Another critical issue of the powered ankle-foot prostheses is that the biomechanics of the human ankle foot should be deeply considered. The torque-angle relationship of the human ankle is nonlinear, especially in the controlled dorsiflexion phase [2], [3], [31]. To mimic the nonlinearity of the torque-angle relationship, different control strategies are needed for the traditional SEA, PEA or SEPA systems [32]–[39]. In addition, some researchers proposed to utilize optimized cam designs [40]–[43] in their actuator system, since the cam can be designed with a specific nonlinear profile. With a nonlinear cam profile, the actuator system does not need to employ a complex controller during the controlled dorsiflexion phase. Based on the biomechanics data from Winter's research [2], we presented a powered ankle-foot prosthesis with a directly driven geared-five bar spring (GFBS) mechanism [44] to better mimic the biomechanics of human ankle during control dorsiflexion phase at normal walking speed in our previous research [45]. Experiments show that the GFBS mechanism can closely mimic the nonlinear torque-angle profile of the able-bodied human ankle due to its rich mechanical features. According to the human biomechanics, the dynamics of the human ankle changes with changing speeds and motion modes. The rich kinematics and dynamics features of the GFB mechanism may bring possibilities to the powered ankle foot prosthesis using the GFBS mechanism for adapting to different speeds or motions by changing the gear ratio or other mechanical parameters [15], [46], [47]. However, the disadvantages of the directly driven actuator and lack of power efficiency optimization leads to that the provided additional energy is insufficient during the powered plantarflexion phase. The user walks very slow to achieve normal gait (0.3Hz) due to the lack of power. As shown in our previous experiment, although it can provide healthy biomechanical features during control dorsiflexion phase, the insufficient features result in a nonsymmetrical gait of the test subject. Hence, in this research, an efficient fully powered ankle-foot prosthesis using theories of the SEA and the GFBS mechanism is presented. By combining the GFBS mechanism and the traditional SEA, a series elastic with geared five-bar (SGFB) actuator is built. The GFBS mechanism is turned into a special SEA by utilizing the theory of variable mechanical parameters [15]. The SGFB actuator has the benefits of both a standard SEA and the GFBS mechanism. Considering the biomechanics of the able-bodied human ankle and the efficiency of the whole prosthesis, the parameters of the actuator system and other parts are optimized to closely mimic the torque-angle profile of a human ankle and reduce the high demand of the motor power. Finally, a preliminary validation experiment is conducted to evaluate the functionality and efficiency of the SGFB prosthesis foot.

The rest of this paper is given as following: Section II describes the modeling and optimization of the SGFB prosthesis foot, Section III presents the mechanical design, electronics and control strategies, Section IV gives the experimental test and evaluation, and Section V concludes the full paper.

II. MODELING AND OPTIMIZATION

A. THE BIOMECHANICS OF THE HUMAN ANKLE

It's very important for the prosthesis designers to understand the biomechanics of the able-bodied human ankle. There are many differences between the biomechanics of human ankle in different daily activities. In this research, the prosthesis is designed for level-ground walking, which is the most common motion in our daily life. According to Winter's research [2], the biomechanics of an able-bodied human ankle are depicted in Fig. 1. A typical ankle gait cycle consists of four distinct phases [48]: Controlled plantarflexion (CP) phase, which starts at the initial contract (IC) of the heel and ends when this foot flat (FF). The ankle angle at IC is set to 0°. During CP phase, the prosthesis foot needs to absorb the impact force and then adapt the human ankle to terrains with different slopes. Controlled dorsiflexion (CD) phase, which starts at FF and ends when the ankle achieves at a maximum dorsiflexion (MD). During CD phase, the prosthesis foot needs to provide vertical support for amputees and stored energy in the elastic component of the SGFB actuator. Powered plantarflexion (PP) phase, which starts at MD and

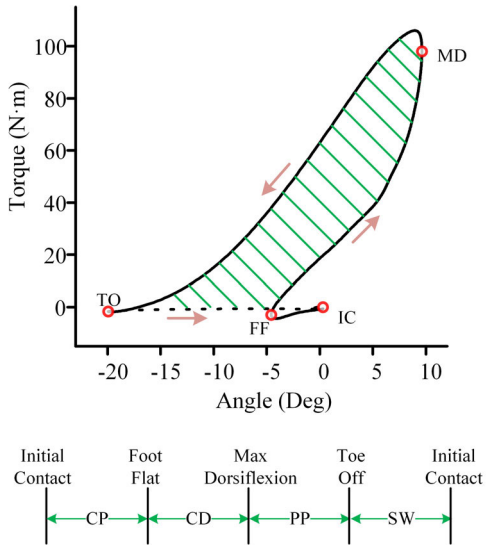

FIGURE 1. The torque-angle profile and the gait phases of a typical able-bodied human ankle (70 kg, 1.25m/s). IC, FF, MD and TO mean initial contact, foot flat, maximum dorsiflexion and toe off respectively. CP, CD, PP, SW mean Controlled plantarflexion, Controlled dorsiflexion, Powered plantarflexion and Swing respectively. The arrows next to the torque-angle curve show the motion direction during an intact walking gait cycle.

ends with toe-off (TO). During PP phase, the prosthesis foot releases the energy stored in the previous phase and needs to provide suitable torque to push-off the human body. The hatched area indicates the net positive work provided by the human ankle during an intact walking gait cycle. Swing (SW) phase, which starts at TO and ends with the next IC. During the SW phase, the prosthesis foot need to be reset for the next IC.

B. ELECTROMECHANICAL MODELING OF THE SGFB PROSTHESIS FOOT

A standard SEA model comprises of a motor, transmissions and a series compliance (see Fig. 2(a)). The compliance is normally implemented as a spring between the output of the transmissions and the load. By using this structure, the actuator system has an increased shock tolerance at heel strike and stores energy when it is providing high resisting torque during the CD phase. The geared five-bar spring mechanism presented in our previous research is depicted in Fig. 2(b). The geared-five bar spring system is composed of five linkages, a parallel spring, a pair of gears fixed on two nonadjacent linkages and five rotary joins. Therefore, the freedom can be calculated from (1). Due to the benefits of abundant design parameters, the geared five-bar spring (GFBS) mechanism can closely replicate the desired nonlinear torque-angle relationship (during the CD phase of walking) after proper optimization.

The SGFB foot is proposed by combining theories of the standard SEA and the GFBS mechanism. As illustrated in Fig. 2(c), the SGFB actuator is formed by using a motor to change the distance $|AE|$ through the implemented transmissions. During an intact walking gait cycle, the change of

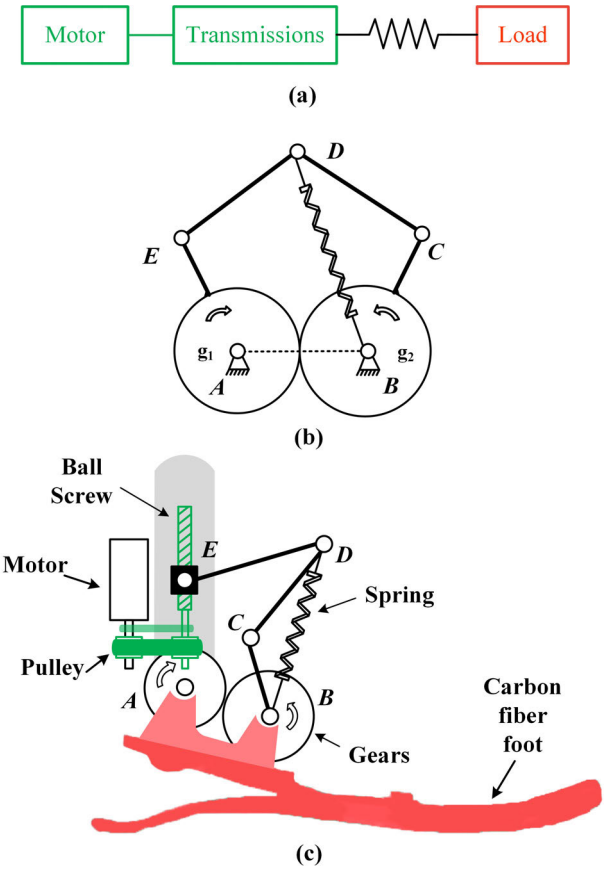

FIGURE 2. The geometric configurations of different models (a) the standard SEA (b) the GFBS mechanism (c) the SGFB actuator. The joint A is selected as the ankle joint. The joint A and B are fixed on a carbon fiber foot.

distance $|AE|$ alters the compression of the series spring and the mathematical equations governing the torque produced around joint A, making the SGFB actuator equivalent to a standard SEA actuator. Then, the torque produced by the GFBS mechanism around the ankle joint A can be changed when the angle $\angle BAE$ remains at a certain value. Hence, the additional energy can be injected to the SGFB foot by the variation of the distance $|AE|$. In this way, the favorable attributes of both the standard SEA and the GFBS mechanism are inherited by the SGFB actuator. Moreover, the complexity of the whole prosthesis foot has been reduced to an acceptable level by the integration of the GFBS mechanism, DC motor and the required transmissions. When we calculate the freedom, the new mechanism can be equivalent to a geared six-bar mechanism consisting of six linkages, a spring, a pair of gears, five rotary joints and one linear joint. Therefore, the freedom of the new mechanism can be derived from (2).

$$n_{\mathrm{GFBS}} = 4 \times 3 - 2 \times 5 - 1 = 1 \tag{1}$$

$$n_{\mathrm{NEW}} = 5 \times 3 - 2 \times 5 - 2 - 1 = 2 \tag{2}$$

In according to the force condition depicted in Fig. 3, the torque produced by the SGFB actuator at ankle joint A can be derived. To simplify the mathematical equations, bar is

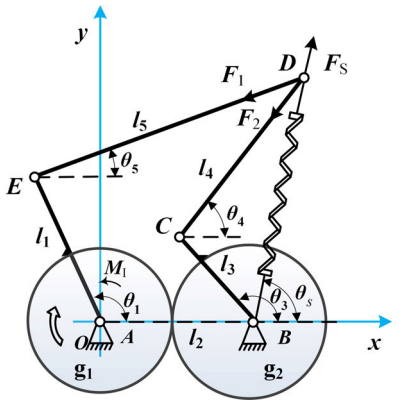

FIGURE 3. The force condition of the SGFB actuator. The distance $|AE|$ (l_1^0) can be changed by the rotation of the DC motor.

placed horizontally. The symbols used in the calculation are defined in Table 1:

The SGFB actuator has its initial status with values of l_1^0, l_S^0 and equilibrium angle θ_1^0, θ_3^0. The equilibrium angle means the angle value when there is no force in the spring. Then, the torque M_I during the whole gait cycle can be derived from the following equations:

$$l_1 = l_1^0 + \Delta x, \theta_1 = \theta_1^0 + \Delta\theta, \theta_3 = \theta_3^0 + \Delta\theta/r \quad (3)$$

$$\theta_5 = \tan^{-1}(\frac{y_C - y_E}{x_C - x_E}) + \cos^{-1}(\frac{l_5^2 + \left|\overrightarrow{EC}\right|^2 - l_4^2}{2l_5\left|\overrightarrow{EC}\right|}) \quad (4)$$

$$x_D = l_1\cos\theta_1 + l_5\cos\theta_5, y_D = l_1\sin\theta_1 + l_5\sin\theta_5 \quad (5)$$

$$F_S = k(l_S - l_S^0) = k(\sqrt{(x_D - x_B)^2 + (y_D - y_B)^2} - l_S^0) \quad (6)$$

$$F_S\sin\theta_S = F_1\sin\theta_5 + F_2\sin\theta_4 \quad (7)$$

$$F_S\cos\theta_S = F_1\cos\theta_5 + F_2\cos\theta_4 \quad (8)$$

$$M_I = F_1 l_1\cos(\theta_1 - \theta_5 - \frac{\pi}{2}) + F_2 l_3\sin(\theta_3 - \theta_4) \quad (9)$$

Once $\Delta\theta$(the ankle angle) and Δx(the change of distance $|AE|$) are known, the torque M_I can be derived by the above equations, which can be rewritten to a function:

$$M_I = \phi(\Delta x, \Delta\theta) \quad (10)$$

The transmissions between the DC motor and Δx composed of a timing pulley (95% efficiency) and a ball screw (90% efficiency). The motor pulley and the ball screw pulley have 22 and 20 teeth respectively. A 2.5mm lead ball screw is used for transforming the rotation of the DC motor to the linear motion of the joint E with high efficiency. Therefore, the torque T_m and displacement θ_m of the motor can be obtained by:

$$T_m = \frac{F_1\cos(\theta_5 - \theta_1 + \pi)}{r_{bs}r_p}\eta, \eta = \begin{pmatrix} \eta_{bs}\times\eta_p (P < 0) \\ \frac{1}{\eta_{bs}\times\eta_p} (P > 0) \end{pmatrix} \quad (11)$$

$$\theta_m = \Delta x \times r_{bs} \times r_p \quad (12)$$

TABLE 1. Symbols used in the electromechanical modeling.

Symbol	Description
$\theta_1, \theta_3, \theta_4, \theta_5$	Angle between the bars and the horizontal line
θ_S	Angle between the spring and the horizontal line
$\Delta\theta$	Ankle angle, which is 0°when the human foot reaches IC
l_1, l_2, l_3, l_4, l_5	Length of the five bars, l_1 means the distance $\|AE\|$specifically
l_s	Length of the spring
F_1, F_2, F_s	Reaction force of bar CD, DE and the spring at joint D
Δx	The change of distance $\|AE\|$
M_I	The torque produced by the SGFB actuator around ankle joint A;
r, r_p, r_{bs}	Gear ratio, timing pulley ratio and the transmission ratio of the ball screw
η_{bs}, η_p	The efficiency of the ball screw and the timing pulley
k	Spring stiffness

According to the electrical full DC motor model [27], [28] and considering that the energy losses caused by inertial torque can be neglected during periodic human walking [49], the electrical power requirement can be determined by:

$$i_m = \frac{v_m\theta_m' + T_m}{k_t} \quad (13)$$

$$v_m = L\frac{di_m}{dt} + R_m i_m + \frac{\theta_m'}{k_b} \quad (14)$$

$$P = i_m v_m \quad (15)$$

where L is the motor's terminal inductance, k_b is the motor's speed constant, k_t is the motor's torque constant, R_m is the motor's terminal resistance and v_m is the motor's damping coefficient value. All these parameters can be obtained and derived from the Maxon motor's datasheet.

C. PARAMETERS OPTIMIZATION

The parameters of the SGFB actuator are optimized to achieve two goals. Firstly, the SGFB actuator has the benefits of the GFBS mechanism to closely mimic the nonlinear torque-angle relationships during the CD phase without complex tracking control. Therefore, in our design, the nonlinear torque angle profile during the CD phase can be replicated by using a certain value of Δx. Secondly, the additional active energy is injected into the prosthesis by changing the distance $|AE|$. During the CP, PP and SW, the distance $|AE|$ has a function of Δx.The parameters of the SGFB actuator and the function Δx need to be optimized to reduce the required motor peak power. Meanwhile, the torque produced by the SGFB actuator also need to mimic the torque angle profile of the human ankle during CP, PP and SW phases. To achieve these two goals, the optimization function is built by discretizing the whole walking gait data into 1000 points,

TABLE 2. Optimal parameters of the SGFB actuator.

Parameters	Values
Initial distance l_1^0 (mm)	29.2
Bar length l_2, l_3, l_4, l_5 (mm)	44.1, 24.9, 65.7, 52.3
Initial equilibrium angle θ_1^0, θ_3^0 (rad)	1.7, 2.6
Gear ratio r	1.75
Spring stiffness k (N/m)	208948
a, b, c	0.41, -0.31, 0.08

shown as following:

$$\Phi(l_1^0, l_2, l_3, l_4, l_5, \theta_1^0, \theta_3^0, r, k, \Delta x) = \frac{1}{1000}\sum_{i=1}^{1000}(T_i - M_{Ii})^2 + \max\{P_i, i = 1 \ldots 1000\} \quad (16)$$

where $l_1^0, l_2, l_3, l_4, l_5, \theta_1^0, \theta_3^0, r, k, \Delta x$ are optimization variables, n is the number of discrete points in CD phase. Once these optimization variables are known, the torque M_{Ii} can be derived by (9). The electrical power P is calculated at each walking gait point. To smooth the function of Δx and simplify the required control, we use a cubic polynomial function to depict the variation of Δx. Then the optimization variable Δx is replaced by a, b, c:

$$\Delta x = ax^3 + bx^2 + cx \quad (17)$$

D. OPTIMIZATION AND SIMULATION RESULTS

The genetic algorithm function in the MATLAB toolbox is used to conduct the optimization. The start points are set according to the optimization experience of the GFBS mechanism. During the optimization, the size constraints are also set to make sure the mechanical design feasibility and compactness. The optimization results are shown in Table 2.

The SGFB actuator is modeled and optimized to closely mimic the torque angle relationships of the intact human ankle. With above optimal values, the simulation results of the SGFB prosthesis foot are illustrated in Fig. 4. To better evaluate the benefits of the SGFB actuator, two strategies named active and semi-active are proposed to be performed in this research. In active strategy, the prosthesis is fully powered and give additional energy during the PP phase. In contrast, the prosthesis adjusts Δx to match the rotation of the ankle joint in the CP phase and doesn't inject energy during PP phase in the semi-active strategy. In both of the two strategies, the prosthesis foot need to be reset to the initial status during the SW phase. The simulation results show that the SGFB prosthesis can replicate the torque angle profiles of the human ankle during the CD phase without complex control by fixing the distance $|AE|$ around a certain value (8mm). In active strategy, with the variation of Δx from 0mm to 60mm, the SGFB actuator can inject enough net active energy into the prosthesis. The peak power of the prosthesis is calculated from the simulation with a value of 146W.

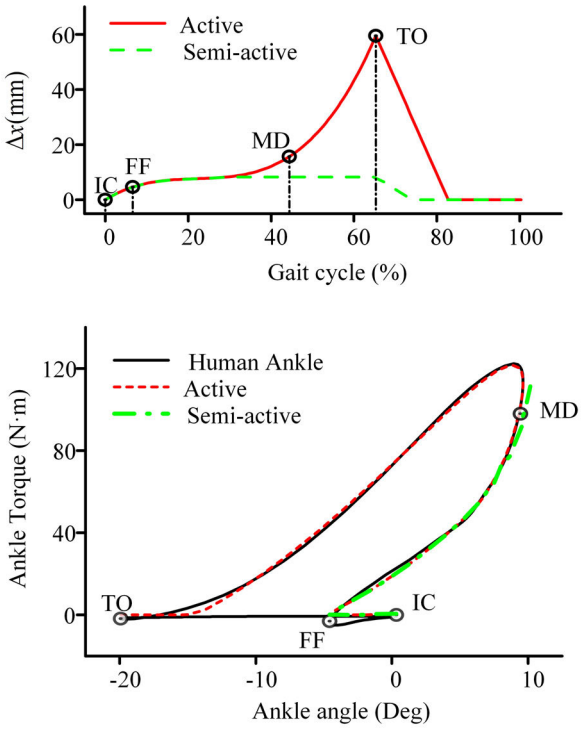

FIGURE 4. The simulation results of the SGFB prosthesis with the active and semi-active strategies.

III. MECHANICAL DESIGN, ELECTRONICS AND CONTROL STRATEGY

A. MECHANICAL IMPLEMENTATION OF THE SGFB PROSTHESIS FOOT

The prototype of the SGFB prosthesis foot contains a SGFB actuator, a carbon fiber foot, a connect tube and an emulator (Fig. 5). The SGFB actuator mainly consists of a GFBS mechanism, a DC motor, a timing pulley and a ballscrew. Considering the requirements of the actuator on torque, speed and peak power, the prosthesis is actuated by a 150W DC motor without gearbox (Maxon motor, Graphite Brushes). A pairs of custom timing pulleys are used to transfer the rotation from the output of the DC motor to the ballscrew (TBI, SFK0802.5, 2.5mm lead). The drive pulley connected to the motor and the pulley driving the ballscrew have 22 and 20 teeth respectively. Hence, the change of Δx can be achieved by the rotation of the implemented DC motor. The GFBS mechanism is made of aluminum alloy and the custom spring is made of spring steel (60Si2MnA) with an initial length of 83mm and a stiffness of 210 N/mm. Considering the behavior of the human ankle during the CP and CD phases, the spring unit is designed to be able to do extension and compression within small mechanical clearance. Therefore, the spring unit can absorb the impact moment around the ankle joint generated at heel strike before the motor adjusts Δx to make the foot flat. In addition, the unique structure of the SGFB prosthesis foot makes it easier to change the spring for different weights of the amputee. The GFBS mechanism is deployed on a carbon fiber foot chosen to absorb the impact force at the heel strike.

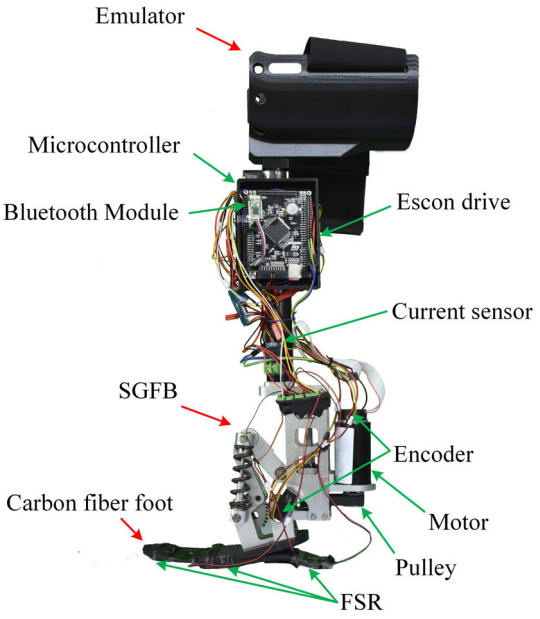

FIGURE 5. The prototype of the SGFB prosthesis foot used in the preliminary experiment. A 3D printed tube is used to connect the SGFB prosthesis foot and the emulator. The DC motor and the ballscrew are fixed on the shank made of aluminum alloy. The microcontroller and ESCON drive are put inside cases fixed on the tube.

The applied embedded electronics are fixed on the shank, which connects the emulator and the prosthesis foot.

B. EMBEDDED ELECTRONICS

The embedded electronic systems (Fig. 6) of the SGFB prosthesis foot include a high-level controller implemented on an embedded board, a low-level current controller for the Maxon DC motor, a signal acquisition and processing system, a communication module and a power module.

A commercial STM32F407ZGT6 micro controller board is chosen to be the main embedded board due to its high frequency clock of 168 MHz with real-time performance, multichannel A/D and D/A converters with high accuracy and abundant ports for communications under different protocols (3 SPI, 3 I2C and 4 USART). The Maxon DC motor is driven by a Maxon current controller ESCON 50/5 which can provide an inner current PID loop (low level control) at 10 kHz. The motor current and motor rotation speed are recorded and sent to the micro controller board by the ESCON drive at 1 kHz. The current to the ESCON drive is also recorded by the micro controller by a current sensor at 1 kHz. Three force sensing resistors (FSR 406) are used to detect the contact between three different sectors of the carbon fiber foot and the ground. The values of the three FSRs will be collected by the micro controller board and converted into the current gait information by the applied finite state machine introduced in the following section. An incremental magnetic rotary encoder (500 turns, 3 channels) is integrated on the DC motor to detect the current rotary position of the DC motor. Another absolute magnetic rotary encoder

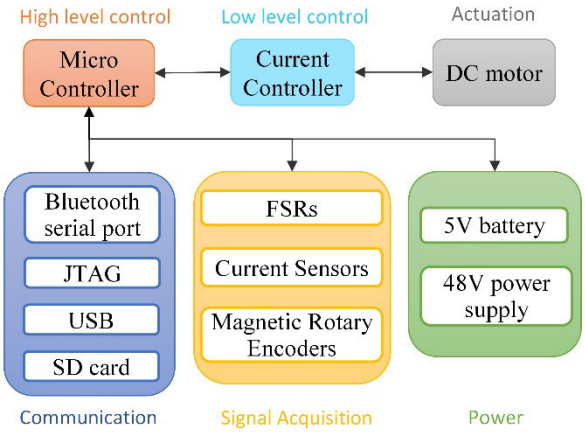

FIGURE 6. Block diagram of the embedded electronic modules within the SGFB prosthesis.

(AMS AS5048A) is deployed on the prosthesis ankle joint to measure the current ankle angle between the shank and the carbon fiber foot.

The ESCON motor driver is powered by a 48V power supply and connected with two long wires. The micro controller, encoders and FSRs are powered by a 5V power module including a power converter module (input 5V-80V to output 5V-20V) and a 7.4V lithium battery. During the experiment, the micro controller communicates with a laptop for starting, ending, reporting error information and adjusting the parameters used in the code of the controller through a Bluetooth module connected with the micro controller by an onboard serial port (Bluetooth Specification4.0BLE, baud rate 115200). The code is downloaded into the micro controller through the JTAG and USB ports. All sensor's data will be recorded in a 32 GB SD card at 250 Hz.

C. TWO CONTROL STRATEGIES WITH FINITE STATE MACHINE

To evaluate the performance of the SGFB prosthesis foot on the torque angle relationships during the CD phase and the energetic features of the actuator during the PP phase, two modes with different control strategies are implemented on the SGFB prosthesis: Semi-active mode and active mode. In both modes, during CP phase, the prosthesis needs to adjust Δx to follow the rotation of the human ankle until the foot flat. During CD phase, the prosthesis stores energy in the series spring and provides the ankle joint the similar torque angle relationships with the human ankle by the GFBS mechanism in the SGFB actuator. As explained in Section II *D*, the difference between the two modes is whether there is positive energy injection during the PP phase. In the active strategy, during the PP phase, the SGFB actuator needs to follow the trajectory of Δx according to the current angle, so that the SGFB prosthesis could provide desired net positive energy to achieve similar torque angle relationships with the human ankle. In the semi-active strategy, during the PP phase, the SGFB prosthesis hold on the position of the motor waiting for the Toe-off. During the SW phase, in both strategies, the

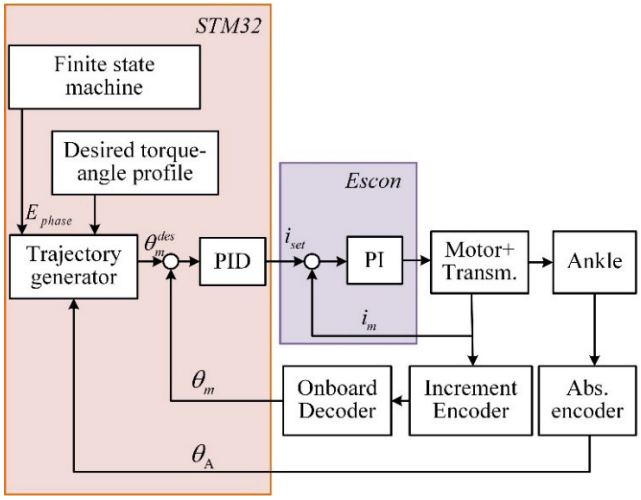

FIGURE 7. The schematics of the controller used within the SGFB prosthesis foot.

TABLE 3. The finite state machnie used in the high-level controller of the SGFB prosthesis foot.

State	Forefoot	Midfoot	Hindfoot	Gait phase
1	OFF	OFF	ON	Early control plantarflexion phase (ECP)
2	OFF	ON	ON	Late control plantarflexion phase (LCP)
3	ON	ON	ON	Control dorsiflexion phase (CD)
4	ON	ON	OFF	Early plantarflexion phase (EPP)
5	ON	OFF	OFF	Late plantarflexion phase (LPP)
6	OFF	OFF	OFF	Swing phase (SW)

On means the sensor are sensing a value greater than the set threshold, while off means the value is less than the threshold.

SGFB actuator needs to be reset to the initial status to prepare for the next heel strike. Several studies use the PD controller [50]–[52] while the classic position PID controller is used as the high-level controller to track the trajectory of Δx in our research, as shown in Fig. 7.

The high-level controller is a classic position PID controller with a position loop at 1 kHz and an inner current loop at 10 kHz. The trajectory generator will generate the next desired angular rotation angle θ_m^{des} of the DC motor based on the desired torque-angle profile, current ankle angle and current gait information. Then the set current i_{set} will be derived and given to the low-level controller implemented on the ESCON drive. The ESCON drive is set as a motor driver with a current loop at 10 kHz. A tuned PI controller is used inside the current loop.

To detect the current phase during normal level ground walking, the finite state machine is used in this research with three FSR sensors attached on the forefoot, midfoot and hindfoot. The finite state machine is illustrated in Table 3.

FIGURE 8. A volunteer wearing the SGFB prosthesis foot through an emulator.

The whole walking gait is divided into 6 phases. Due to the using of an FSR sensor on the midfoot, the CP and PP phase can be separated into early and late phases. Then, combining with the sensor information about the current ankle angle, the controller might get more detailed information about the current walking gait and improve the dynamic performance.

IV. EXPERIMENTAL TEST AND EVALUATION

The experiment is conducted on a treadmill with an able-bodied volunteer wearing an emulator [53]–[57], as shown in Fig. 8. The treadmill experiment can preliminarily evaluate the performance of the SGFB prosthesis on dynamic characteristics and energetics.

A. PARAMETERS TUNING

Before conducting the test on the treadmill, the parameters of the high-level controller and the low-level controller need to be tuned to closely track the trajectory of Δx. The proportional and integral values of the PI controller in the current loop is auto tuned by the Maxon ESCON studio, which has been used and proved to be efficient in several studies. The proportional, integral and derivative values of the PID controller in the position control loop is tuned during the experiment. Due to the kinetic and kinematics of the human ankle, the requirements of the controller in different phases are quite different. In our research, the PID parameters are tuned for all phases respectively. In the CP phase, the prosthesis needs to quickly follow the rotation of the human ankle with a quite small torque during the movement. In the CD phase, the controller needs to hold on the position of the DC motor. The Position PID controller is changed into an efficient simple PI controller by setting a high proportional value, low integral value and 0 differential value. In the PP phase, the motor needs to inject active energy to the prosthesis. Hence, the values of the PID controller is tuned iteratively by our experience on PID turning. The PID controller is initially set with a soft impedance. Then the proportional value and integral values are increased with increasing controller impedance. Considering the trajectory of Δx and the kinematics of the volunteer, the PID parameters for the PP phase are carefully tuned after a week online tuning. During the tuning process, the volunteer is walking on the treadmill with our emulator system at 1.2m/s. In the

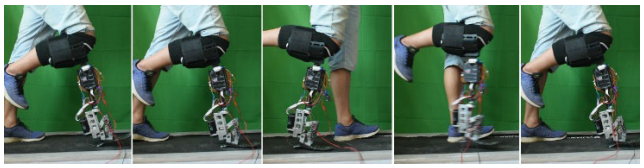

FIGURE 9. The walking trial conducted on a treadmill with a volunteer wearing the SGFB prosthesis through an emulator.

SW phase, the prosthesis is quickly and precisely reset to the initial status. Besides, small overshoot is permitted during this tuning process. The parameters of the PID controller for all phases are recorded in the high-level controller implemented on the embedded board STM32F407ZGT6.

When switching between different phases, the PID gains need to be set specifically and the integral term will be set to 0. From the CP phase to the CD phase, the switching causes slight shock since the required torque during the CP phase is very small. From the CD phase to the PP phase, the integral term is set to a tuned value after setting the PID gains to reduce the amplitude and duration time of the shock. From the PP phase to the SW phase, there is no heavy shock in the switching process since the ankle torque is also very small when the Toe Off is detected. In the late SW phase, the PID gains will be set for the next CP phase after the ankle foot has been reset to the initial status without any torque around the ankle joint. Therefore, the problem caused by switching PID gains between different phases is alleviated to an acceptable level.

B. WALKING TEST ON THE TREADMILL

With the tuned parameters of the two controllers, the subject walks with the SGFB prosthesis foot on the treadmill where the speed is set at 1.2m/s. A high-speed camera (Logitech, 1920∗1080 150fps) is used to capture the walking locomotion. After two weeks training, the subject can comfortably walk with the SGFB prosthesis foot through the emulator system. Then, six trials are conducted where the subject needs to walk for 5 minutes in each experimental trial. The SGFB prosthesis are evaluated in two modes where each mode comprises of three trials. Fig. 9 shows an intact walking cycle of the amputee wearing the SGFB prosthesis on the treadmill. The sensor data during six trials are collected by the integrated signal acquisition system and recorded in the onboard SD card. The motor angular position θ_m is recorded by the integrated incremental magnetic encoder and the change of the ankle angle $\Delta\theta$ is recorded by the integrated absolute magnetic encoder. Then the torque provided by the SGFB prosthesis foot at the ankle joint can be derived by (10).

Fig. 10(a) shows the comparison of the referenced able-bodied human ankle and the SGFB prosthesis foot on torque versus ankle angle curve during an intact walking gait cycle in the preliminary experiment walking test. The results indicate that the torque angle relationship produced by the SGFB prosthesis foot is similar to that of the able-bodied human ankle during the whole walking gait cycle in the active mode.

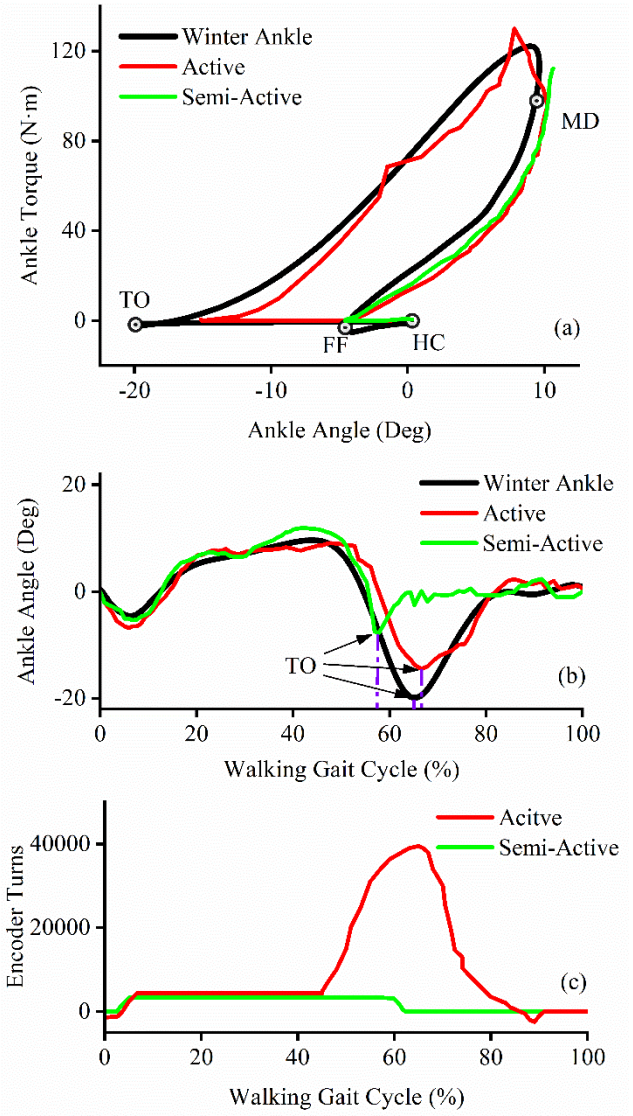

FIGURE 10. The experiment results of the SGFB prosthesis foot walking on the treadmill. (a) the torque angle relationship, (b) the ankle angle, (c) the angular position of the Maxon RE40 motor. The toe-off is pointed by arrows in (b).

This means the SGFB actuator can inject desired positive energy during PP phase. In both semi-active mode and active mode, the SGFB prosthesis can provide healthy torque features as we optimized and designed during the CP phase and CD phase. It should be noticed that, from FF to MD, the torque produced by the SGFB prosthesis foot is slightly smaller than that of the human ankle. This is due to the mechanical clearance existed in the mechanical transmission systems, especially in the gears and the pulleys. Compared with the ideal desired torque angle relationships, the torque of the SGFB prosthesis foot with the applied high-level controller increases sharply when the heel off is detected after MD. Then the torque decreases to be 10 Nm smaller than the referenced data until the ankle angle reaches at $-4°$.

Fig. 10(b) shows the recorded data of the ankle angle collected by the AS5048 absolute magnetic encoder mounted

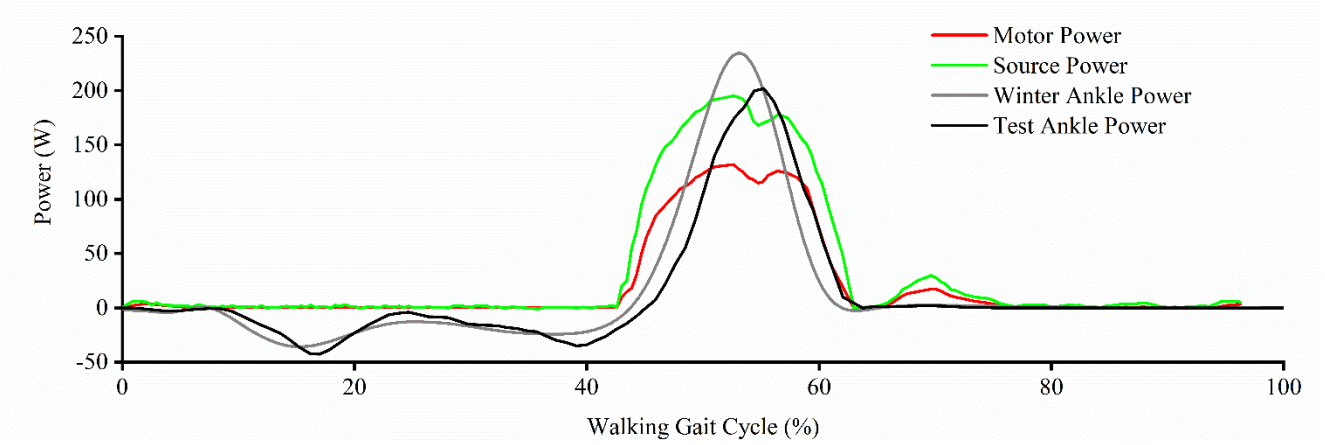

FIGURE 11. The power at different measured points during the whole walking gait cycle. The gray line depicts the ankle power calculated from Winter's data. The motor power and the source power are the electrical power measured at the motor and source point. The test ankle power and the Winter ankle power means the mechanical ankle power of the tested subject and the subjects in Winter's research respectively.

between the shank and the carbon-fiber foot. The ankle angle is used to evaluate the walking gait. The normal walking gait means the ankle angle of the volunteer is similar to that of the averaged able-bodied human ankle data. It can be known that the subject wearing the SGFB prosthesis foot in semi-active mode has a smaller range of the ankle angle from $-6°$ to $12°$, compared with that of the able-bodied human ankle. This abnormal walking gait is due to the insufficient energy feature during the PP phase. Compared with the semi-active mode, the active mode enables the SGFB prosthesis foot to provide the subject a better walking gait when we look at the ankle angle of the volunteer and the referenced data. In the active mode, the rotation range of the ankle angle is from -13° to 11°. Compared with the semi-active mode, the active mode increased the range of the ankle angle by 6 degrees by injecting positive energy during PP phase. The difference of the ankle angle of the subject wearing the SGFB prosthesis foot in active mode with the referenced data may due to the individual diversity between the subject in this research and the subjects in Winter's research. Another important phenomenon (labeled in Fig. 10(b)) is that the subject wearing the SGFB prosthesis foot in semi-active mode reaches TO earlier at 57% of the walking gait cycle when compared with the able-bodied human ankle reaching TO at 65% and with the SGFB prosthesis in the active mode reaching TO at 68%. This means the energy features of the human ankle will change the distribution of different gait phases in the whole walking gait. The insufficient energy feature of the semi-active mode will shorten the PP phase. Besides, the torque angle relationship of the SGFB prosthesis foot provides the subject a similar walking gait with the able-bodied human during the CP phase and CD phase in both semi-active mode and active mode.

Fig. 10(c) shows the angular position of the Maxon RE40 DC motor. The high-level controller enables the actuator to approximately track the desired trajectory of Δx depicted in Figure 4. It can be clearly seen that, the SGFB prosthesis in semi-active mode reaches TO earlier than that in active mode. Besides, the high-level controller can effectively reset the SGFB prosthesis foot to the initial status with a small overshoot at 88% of the walking gait.

C. POWER TRANSFERRING AND ENERGY CONSUMPTION

One of the main design principles of the SGFB prosthesis foot is to inject enough positive energy during PP phase by improving the efficiency of the actuator system. The previous section has proven that the SGFB prosthesis foot in active mode can approximately mimic the behavior of the able-bodied human ankle by injecting additional energy during different phases. In this research, the source power of the whole prosthesis system P_S, the motor electrical power P_E and the actual output power of the ankle joint P_A are calculated to evaluate the performance of the optimization process on reducing the required peak power by improving the efficiency of the actuator system. The programmable power supply is set to 48V considering the nominal voltage of the Maxon RE40 is 48V. The current from the programmable power supply to the ESCON drive is measured by a current sensor (ACS712, 0-5A) and recorded at 1 kHz. As described in section 3.2, the motor current and speed are outputted by the ESCON drive. Then, the motor voltage v_m can be derived from (14). The torque at the ankle joint is derived in Section IV.B. The rotation speed θ'_A of the ankle joint is calculated by the derivation of the ankle angle recorded by the magnetic absolutely encoder AS5048A. From these parameters, the source power of the whole prosthesis system P_S, the motor electrical power P_E and the actual output mechanical power of the ankle joint (test ankle power) P_A can be calculated by multiplying the corresponding voltage and current or torque and rotation speed during the whole walking gait cycle, as shown in Fig. 11.

Compared with the referenced Winter data, the test subject shows similar peak power and positive energy requirement during the walking gait cycle. The detailed values of the

TABLE 4. Peak power and energy consumption.

Measured Point	Peak Power W	Energy J	Efficiency %
Source Power	195	38.5	100
Motor Power	132	24.4	63.4
Test Ankle Power	202	13.6	35.3
Winter Ankle Power	234.4	15.5	

The peak power is the average of the maximum power during every stride performed in the three trials where the SGFB prosthesis foot is set to the active mode, the energy is derived by integrating the power over all the strides and divided by the number of the strides, the efficiency is the ratio of the energy measured at the current point and the energy measured at the source power point.

peak power and energy consumption are listed in Table 4. To provide the amputee with similar walking gait, the SGFB prosthesis foot needs to generate 202 W power at the ankle joint and inject 13.6 J net positive energy. The 13.6 J net positive energy is provided by the whole SGFB prosthesis foot with an energy efficiency of 35.3%. The peak power of the motor is reduced by 34% from 202 W of the ankle joint to 132 W of the Maxon RE40 motor. The decrease of the peak power of the motor from 146W in simulation to 132W in experimental trials may due to the using of the hand to keep balance during the walking gait. It should be noticed that, the programmable power supply still needs to provide a peak power of 195 W and an energy consumption of 38.5 J. The use of the ESCON driver and the Maxon RE40 motor leads to an energy efficiency of 63.4%, which is acceptable compared with other actuator systems applied in the active prosthetic systems.

In [26], the motor need to consume around 5W to hold on the motor position in the CD phase under 110Nm ankle torque. However, our prosthesis consume 2W to hold on the position. This is due to the friction force existed in the transmissions and the GFBS system is bigger than that of [26]. Therefore, only small power is detected after using of a filter to smooth the curve.

D. EFFICIENCY EVALUATION OF THE MOTOR

In order to clearly evaluate the benefits of the optimization process on reducing the peak power of the actuator system by considering the efficiency of every parts within the whole active prosthesis system and using of the new SGFB actuator system, the motor current and speed during the treadmill trials are depicted in Fig. 12(a) and (b). The Maxon RE40 DC motor reaches a maximum current of 3.3 A and a maximum speed of 5447 rpm, which is under its limits for continuous operation. Furthermore, the motor torque and the motor speed are visualized on an power efficiency map in Fig. 12(c), according the methods of modeling of geared DC motor for power efficiency [27]. To evaluate the power efficiency of the DC motor at high power condition, we labeled the trajectory of the motor torque and the motor speed with a power over 70W during the treadmill walking trial. It can be clearly seen that the DC motor operates at the high efficiency area (over 70%) when the power of the motor is larger than 70 W. This shows the benefits of the optimization process.

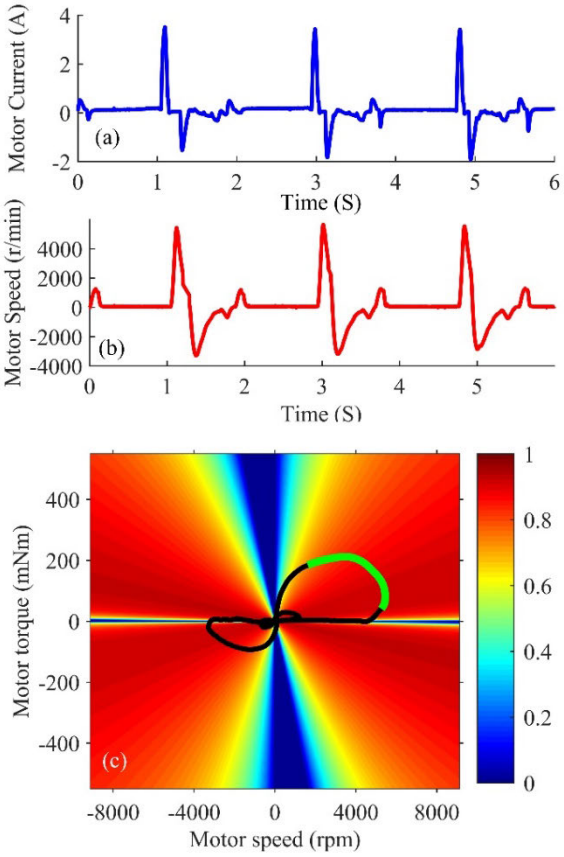

FIGURE 12. The current and speed of the Maxon RE40 motor during several walking gait cycle in the treadmill trial. (a) and (b) depict the motor current and motor speed during several walking gait cycles. (c) visualizes the motor torque and speed on an efficiency map of the Maxon RE40 motor. The operation of the motor is labeled by the green color while the motor power is larger than 70W.

By considering the efficiency of every parts within the whole active prosthesis system and using of the new SGFB actuator system, the peak power can be reduced by improving the efficiency of the DC motor when it's providing high power output.

V. CONCLUSION

In this research, the authors proposed the SGFB actuator for the active prosthesis foot based on the geared five-bar spring system. The SGFB actuator has the benefits of both the SEA actuator and the GFBS mechanism and is able to approximately mimic the biomechanics of the human ankle and reduce electrical motor requirements. The experiment results of the prototype of the SGFB prosthesis foot show that the SGFB prosthesis foot provides the test subject biomechanics similar to the referenced Winter data. Both the semi-active mode and the active mode can provide healthy biomechanics during the CD phase. The lack of positive energy injection in semi-active mode leads to a change in walking gait, especially the distribution of different phases and a reduction of ankle plantarflexion during an intact walking gait cycle. This also demonstrates the importance of providing net positive energy in prosthetic feet. Furthermore, the experiments of the SGFB

prosthesis foot will be conducted on lower-limb amputees to furthermore evaluate the performance of the whole prosthesis foot system in the future.

By considering the efficiency of every part within the SGFB prosthetic foot, the electromechanical model of the whole prosthesis system is built. Thanks to the optimization of different parameters with the electromechanical model on reducing the peak power, the SGFB actuator can provide enough positive energy during the whole walking gait cycle with an energy efficiency of 63.4%. This leads to a normal walking gait during the level ground walking on a treadmill at 1.2m/s. The experimental trajectory of the motor torque and the motor speed on an power efficiency map of the DC motor indicates that the efficiency of the actuator is improved by operating the high-power tasks (over 70W) in the high efficiency area of the motor. It should be noticed that even though the peak power of the DC motor has been effectively reduced to 132 W, the whole prosthesis system still has an overall energy efficiency of only 35.3%. In long-time daily using condition, this will lead to a high battery capacity requirement. How to handle the tread-off on reducing the peak power and the energy consumption of the SGFB prosthetic foot will be studied in the future. In total, the design, optimization of the new prosthesis improved the performance when we compared it to our previous design. The previous one can only mimic the walking gait very slowly due to the insufficient design of the actuator system. Besides, the control strategy provide the prosthesis potential adaptability to terrains with different slopes in the CP phase. The overall energy efficiency also show that the efficiencies of the ball screw and the timing pulley may be lower than the given value. Considering that, the transmission system should be more detailed calculated and modeled in the next generation prosthesis.

As shown in Fig. 10, there is difference between the experiment results with the Winter's data. However, the volunteer gives very positive feedback about the prosthesis that it can give stable support and suitable pushing effort. The walking frequency (0.6Hz) is slightly lower than normal people (0.7-0.8Hz), but it is still acceptable. Therefore, the difference in Fig. 10 may due to the difference between different people's walking gait. Hence, the control parameters and the spring stiffness need to be tuned for different users. Furthermore, the SGFB prosthesis foot also shows other limitations due to its mechanical performance. The gears and pulleys lead to mechanical play when the rotation of the ankle angle is reversed. In the preliminary experimental trials, the mechanical parts around the gears get worn easily after the first 50 hours of the operation. Then, the mechanical play becomes completely unacceptable when the SGFB prosthesis foot has been used for 100 hours continuously without overhaul. Hence, the mechanical structure of the SGFB prosthesis foot will be totally optimized to make it lighter and more reliable.

REFERENCES

[1] H. Masum, S. Bhaumik, and R. Ray, "Conceptual design of a powered ankle-foot prosthesis for walking with inversion and eversion," *Procedia Technol.*, vol. 14, pp. 228–235, Jan. 2014.

[2] D. A. Winter, "Kinematic and kinetic patterns in human gait: Variability and compensating effects," *Hum. Movement Sci.*, vol. 3, nos. 1–2, pp. 51–76, Mar. 1984.

[3] G. Bovi, M. Rabuffetti, P. Mazzoleni, and M. Ferrarin, "A multiple-task gait analysis approach: Kinematic, kinetic and EMG reference data for healthy young and adult subjects," *Gait Posture*, vol. 33, no. 1, pp. 6–13, 2011.

[4] C. L. Vaughan, B. L. Davis, and J. C. O'Connor, *Dynamics of Human Gait*. Champaign, IL, USA: Human Kinetics Publishers, 1992.

[5] S. Debta and K. Kumar, "Biomedical design of powered ankle-foot prosthesis—A review," *Mater. Today, Proc.*, vol. 5, no. 2, pp. 3273–3282, 2018.

[6] J. Andrysek, "Lower-limb prosthetic technologies in the developing world: A review of literature from 1994–2010," *Prosthetics Orthotics Int.*, vol. 34, no. 4, pp. 378–398, Dec. 2010.

[7] P. Cherelle, G. Mathijssen, Q. Wang, B. Vanderborght, and D. Lefeber, "Advances in propulsive bionic feet and their actuation principles," *Adv. Mech. Eng.*, vol. 6, Jan. 2014, Art. no. 984046.

[8] T. Yu, A. Plummer, P. Iravani, J. Bhatti, S. Zahedi, and D. Moser, "The design, analysis and testing of a compact electrohydrostatic powered ankle prosthesis," in *Proc. BATH/ASME Symp. Fluid Power Motion Control*, Sep. 2016, pp. 1–7.

[9] M. Cempini, L. J. Hargrove, and T. Lenzi, "Design, development, and bench-top testing of a powered polycentric ankle prosthesis," in *Proc. IEEE/RSJ Int. Conf. Intell. Robots Syst. (IROS)*, Sep. 2017, pp. 1064–1069.

[10] S. K. Au, H. Herr, J. Weber, and E. C. Martinez-Villalpando, "Powered ankle-foot prosthesis for the improvement of amputee ambulation," in *Proc. 29th Annu. Int. Conf. IEEE Eng. Med. Biol. Soc.*, Aug. 2007, pp. 3020–3026.

[11] J. Zhu, Q. Wang, and L. Wang, "PANTOE 1: Biomechanical design of powered ankle-foot prosthesis with compliant joints and segmented foot," in *Proc. IEEE/ASME Int. Conf. Adv. Intell. Mechatronics*, Jul. 2010, pp. 31–36.

[12] Z. Safaeepour, A. Esteki, F. T. Ghomshe, and M. E. Mousavai, "Design and development of a novel viscoelastic ankle-foot prosthesis based on the human ankle biomechanics," *Prosthetics Orthotics Int.*, vol. 38, no. 5, pp. 400–404, Oct. 2014.

[13] B. J. Bergelin and P. A. Voglewede, "Design of an active ankle-foot prosthesis utilizing a four-bar mechanism," *J. Mech. Des.*, vol. 134, no. 6, Jun. 2012, Art. no. 061004.

[14] E. J. Rouse, N. C. Villagaray-Carski, R. W. Emerson, and H. M. Herr, "Design and testing of a bionic dancing prosthesis," *PLoS ONE*, vol. 10, no. 8, 2015, Art. no. e0135148.

[15] D. Dong, B. Convens, Y. Sun, W. Ge, P. Cherelle, and B. Vanderborght, "The effects of variable mechanical parameters on peak power and energy consumption of ankle-foot prostheses at different speeds," *Adv. Robot.*, vol. 32, no. 23, pp. 1229–1240, Dec. 2018.

[16] M. Eslamy, M. Grimmer, and A. Seyfarth, "Effects of unidirectional parallel springs on required peak power and energy in powered prosthetic ankles: Comparison between different active actuation concepts," in *Proc. IEEE Int. Conf. Robot. Biomimetics (ROBIO)*, Dec. 2012, pp. 2406–2412.

[17] R. Ham, T. Sugar, B. Vanderborght, K. Hollander, and D. Lefeber, "Compliant actuator designs," *IEEE Robot. Autom. Mag.*, vol. 16, no. 3, pp. 81–94, Sep. 2009.

[18] B. Vanderborght *et al.*, "Variable impedance actuators: A review," *Robot. Auto. Syst.*, vol. 61, no. 12, pp. 1601–1614, Dec. 2013.

[19] J. K. Hitt, T. G. Sugar, M. Holgate, and R. Bellman, "An active foot-ankle prosthesis with biomechanical energy regeneration," *J. Med. Devices*, vol. 4, no. 1, Mar. 2010, Art. no. 011003.

[20] J. K. Hitt, R. Bellman, M. Holgate, T. G. Sugar, and K. W. Hollander, "The sparky (spring ankle with regenerative Kinetics) project: Design and analysis of a robotic transtibial prosthesis with regenerative Kinetics," in *Proc. ASME Int. Design Eng. Tech. Conf. Comput. Inf. Eng. Conf.*, 2007, pp. 1587–1596.

[21] G. Pratt and M. M. Williamson, "Series elastic actuators," in *Proc. IEEE/RSJ Int. Conf. Intell. Robots Syst. 'Hum. Robot Interact. Cooperat. Robots'*, vol. 1, Aug. 1995, pp. 399–406.

[22] S. H. Collins, M. Kim, T. Chen, and T. Chen, "An ankle-foot prosthesis emulator with control of plantarflexion and inversion-eversion torque," in *Proc. IEEE Int. Conf. Robot. Autom. (ICRA)*, May 2015, pp. 1210–1216.

[23] M. Grimmer, M. Holgate, J. Ward, A. Boehler, and A. Seyfarth, "Feasibility study of transtibial amputee walking using a powered prosthetic foot," in *Proc. Int. Conf. Rehabil. Robot. (ICORR)*, Jul. 2017, pp. 1118–1123.

[24] H. M. Herr and A. M. Grabowski, "Bionic ankle-foot prosthesis normalizes walking gait for persons with leg amputation," *Proc. Roy. Soc. London B, Biol. Sci.*, vol. 279, no. 1728, pp. 457–464, 2012.
[25] F. Gao, W.-H. Liao, B. Chen, H. Ma, and L.-Y. Qin, "Design of powered ankle-foot prosthesis driven by parallel elastic actuator," in *Proc. IEEE Int. Conf. Rehabil. Robot. (ICORR)*, Aug. 2015, pp. 374–379.
[26] B. Convens, D. Dong, R. Furnemont, T. Verstraten, P. Cherelle, D. Lefeber, and B. Vanderborght, "Modeling, design and test-bench validation of a semi-active propulsive ankle prosthesis with a clutched series elastic actuator," *IEEE Robot. Autom. Lett.*, vol. 4, no. 2, pp. 1823–1830, Apr. 2019.
[27] T. Verstraten, G. Mathijssen, R. Furnémont, B. Vanderborght, and D. Lefeber, "Modeling and design of geared DC motors for energy efficiency: Comparison between theory and experiments," *Mechatronics*, vol. 30, pp. 198–213, Sep. 2015.
[28] T. Verstraten, R. Furnémont, G. Mathijssen, B. Vanderborght, and D. Lefeber, "Energy consumption of geared DC motors in dynamic applications: Comparing modeling approaches," *IEEE Robot. Autom. Lett.*, vol. 1, no. 1, pp. 524–530, Jan. 2016.
[29] E. J. Rouse, L. M. Mooney, and H. M. Herr, "Clutchable series-elastic actuator: Implications for prosthetic knee design," *Int. J. Robot. Res.*, vol. 33, no. 13, pp. 1611–1625, Nov. 2014.
[30] M. Grimmer and A. Seyfarth, "Stiffness adjustment of a series elastic actuator in an ankle-foot prosthesis for walking and running: The trade-off between energy and peak power optimization," in *Proc. IEEE Int. Conf. Robot. Autom. (ICRA)*, May 2011, pp. 1439–1444.
[31] H. Bateni and S. J. Olney, "Kinematic and kinetic variations of below-knee amputee gait," *J. Prosthetics Orthotics*, vol. 14, no. 1, pp. 2–10, Mar. 2002.
[32] N. Paine, S. Oh, and L. Sentis, "Design and control considerations for high-performance series elastic actuators," *IEEE/ASME Trans. Mechatronics*, vol. 19, no. 3, pp. 1080–1091, Jun. 2014.
[33] D. Ragonesi, S. Agrawal, W. Sample, and T. Rahman, "Series elastic actuator control of a powered exoskeleton," in *Proc. Annu. Int. Conf. IEEE Eng. Med. Biol. Soc.*, Aug. 2011, pp. 3515–3518.
[34] J. Bae, K. Kong, and M. Tomizuka, "Gait phase-based smoothed sliding mode control for a rotary series elastic actuator installed on the knee joint," in *Proc. Amer. Control Conf.*, Jun. 2010, pp. 6030–6035.
[35] I. Thorson and D. Caldwell, "A nonlinear series elastic actuator for highly dynamic motions," in *Proc. IEEE/RSJ Int. Conf. Intell. Robots Syst.*, Sep. 2011, pp. 390–394.
[36] J. Austin, A. Schepelmann, and H. Geyer, "Control and evaluation of series elastic actuators with nonlinear rubber springs," in *Proc. IEEE/RSJ Int. Conf. Intell. Robots Syst. (IROS)*, Sep. 2015, pp. 6563–6568.
[37] A. Calanca and P. Fiorini, "Human-adaptive control of series elastic actuators," *Robotica*, vol. 32, no. 8, pp. 1301–1316, Dec. 2014.
[38] P. Beckerle, J. Wojtusch, J. Schuy, B. Strah, S. Rinderknecht, and O. V. Stryk, "Power-optimized stiffness and nonlinear position control of an actuator with variable torsion stiffness," in *Proc. IEEE/ASME Int. Conf. Adv. Intell. Mechatronics*, Jul. 2013, pp. 387–392.
[39] M. Hutter, C. D. Remy, and R. Siegwart, "Design of an articulated robotic leg with nonlinear series elastic actuation," in *Mobile Robotics: Solutions and Challenges*. Singapore: World Scientific, 2010, pp. 645–652.
[40] F. Gao, Y. Liu, and W.-H. Liao, "Design of powered ankle-foot prosthesis with nonlinear parallel spring mechanism," *J. Mech. Des.*, vol. 140, no. 5, May 2018, Art. no. 055001.
[41] J. Realmuto, G. Klute, and S. Devasia, "Nonlinear passive cam-based springs for powered ankle prostheses," *J. Med. Devices*, vol. 9, no. 1, Mar. 2015, Art. no. 011007.
[42] C. Copilusi, N. Dumitru, L. Rusu, and M. Marin, "Cam mechanism kinematic analysis used in a human ankle prosthesis structure," in *Proc. World Congr. Eng.*, London, U.K., Jun. 2010, pp. 1316–1320.
[43] T. Lenzi, M. Cempini, J. Newkirk, L. J. Hargrove, and T. A. Kuiken, "A lightweight robotic ankle prosthesis with non-backdrivable cam-based transmission," in *Proc. Int. Conf. Rehabil. Robot. (ICORR)*, Jul. 2017, pp. 1142–1147.
[44] Y. Sun, W. Ge, J. Zheng, and D. Dong, "Design and evaluation of a prosthetic knee joint using the geared five-bar mechanism," *IEEE Trans. Neural Syst. Rehabil. Eng.*, vol. 23, no. 6, pp. 1031–1038, Nov. 2015.
[45] D. Dong, W. Ge, S. Liu, F. Xia, and Y. Sun, "Design and optimization of a powered ankle-foot prosthesis using a geared five-bar spring mechanism," *Int. J. Adv. Robot. Syst.*, vol. 14, no. 3, May 2017, Art. no. 172988141770454.
[46] I. A. Sultan and A. Kalim, "On the kinematics and synthesis of a geared five-bar slider–crank mechanism," *Proc. Inst. Mech. Eng. C, J. Mech. Eng. Sci.*, vol. 225, no. 5, pp. 1253–1261, May 2011.
[47] D. Mundo, G. Gatti, and D. B. Dooner, "Optimized five-bar linkages with non-circular gears for exact path generation," *Mechanism Mach. Theory*, vol. 44, no. 4, pp. 751–760, Apr. 2009.
[48] M. L. Palmer, "Sagittal plane characterization of normal human ankle function across a range of walking gait speeds," Ph.D. dissertation, Massachusetts Inst. Technol., Cambridge, MA, USA, 2002.
[49] E. A. B. Nieto, S. Rezazadeh, and R. D. Gregg, "Minimizing energy consumption and peak power of series elastic actuators: A convex optimization framework for elastic element design," *IEEE/ASME Trans. Mechatronics*, vol. 24, no. 3, pp. 1334–1345, Jun. 2019.
[50] D. Quintero, D. J. Villarreal, and R. D. Gregg, "Preliminary experiments with a unified controller for a powered knee-ankle prosthetic leg across walking speeds," in *Proc. IEEE/RSJ Int. Conf. Intell. Robots Syst. (IROS)*, Oct. 2016, pp. 5427–5433.
[51] J. Park, G.-H. Yoon, J.-W. Kang, and S.-B. Choi, "Design and control of a prosthetic leg for above-knee amputees operated in semi-active and active modes," *Smart Mater. Struct.*, vol. 25, no. 8, Aug. 2016, Art. no. 085009.
[52] J.-H. Kim and J.-H. Oh, "Development of an above knee prosthesis using MR damper and leg simulator," in *Proc. IEEE Int. Conf. Robot. Autom. (ICRA)*, vol. 4, May 2001, pp. 3686–3691.
[53] S. K. Au, P. Dilworth, and H. Herr, "An ankle-foot emulation system for the study of human walking biomechanics," in *Proc. IEEE Int. Conf. Robot. Autom. (ICRA)*, May 2006, pp. 2939–2945.
[54] H. Zhao, E. Ambrose, and A. D. Ames, "Preliminary results on energy efficient 3D prosthetic walking with a powered compliant transfemoral prosthesis," in *Proc. IEEE Int. Conf. Robot. Autom. (ICRA)*, May 2017, pp. 1140–1147.
[55] Y. Sun, P. Tang, J. Zheng, D. Dong, X. Chen, L. Bai, and W. Ge, "Optimal design of a nonlinear series elastic actuator for the prosthetic knee joint based on the conjugate cylindrical cam," *IEEE Access*, vol. 7, pp. 140846–140859, 2019.
[56] Y. Wen, M. Liu, J. Si, and H. H. Huang, "Adaptive control of powered transfemoral prostheses based on adaptive dynamic programming," in *Proc. 38th Annu. Int. Conf. IEEE Eng. Med. Biol. Soc. (EMBC)*, Aug. 2016, pp. 5071–5074.
[57] R. D. Gregg, T. Lenzi, N. P. Fey, L. J. Hargrove, and J. W. Sensinger, "Experimental effective shape control of a powered transfemoral prosthesis," in *Proc. IEEE 13th Int. Conf. Rehabil. Robot. (ICORR)*, Jun. 2013, pp. 1–7.

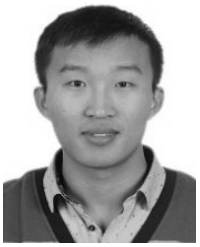

DIANBIAO DONG received the B.S. degree in mechanical engineering from Northwestern Polytechnical University, in 2013, where he is currently pursuing the Ph.D. degree. Since 2016, he has been a joint Ph.D. Student with the Department of Mechanical Engineering (MECH), Vrije Universiteit Brussel.

His research interests include design, actuation, and control of the ankle-foot prosthetics, exoskeleton, and bionic robotics.

WENJIE GE received the B.S. degree in mechanical design and manufacturing from the Xi'an University of Technology, and the M.S. and Ph.D. degrees in mechanical engineering from Northwestern Polytechnical University.

He is currently a Professor with Northwestern Polytechnical University. His research interests include mechanical theory and mechanism, mechanical dynamics, robotic mechanism, and bionic robotics.

BRYAN CONVENS received the master's degree in electromechanical engineering from Vrije Universiteit Brussel (VUB) and the Université Libre de Bruxelles (ULB), in 2016. He is currently pursuing the Ph.D. degree funded by the Research Foundation Flanders—Fonds Wetenschappelijk Onderzoek (FWO) with the Robotics and Multibody Mechanics Research Group, VUB.

His research interest includes the theory and application of model-based computationally efficient control strategies for robotics with strong safety and performance guarantees.

YUANXI SUN received the B.S. and Ph.D. degrees in mechanical engineering from Northwestern Polytechnical University, Xi'an, Shaanxi, China, in 2011 and 2017, respectively.

He is currently with the College of Mechanical Engineering, Chongqing University, Chongqing, China. His research interests include design, actuation, and control of lower limb prosthesis, exoskeleton, and bionic robotics.

TOM VERSTRATEN received the master's degree in electromechanical engineering and the Ph.D. degree from Vrije Universiteit Brussel (VUB), in 2012 and 2018, respectively.

In January 2020, he has appointed as a Professor at VUB. His research interest includes the study and development of energy-efficient actuators incorporating compliance and redundancy.

BRAM VANDERBORGHT received the Ph.D. degree, in 2007.

In 2006, he performed research on the humanoids robot HRP-2 with AIST, Tsukuba, Japan. From October 2007 to April 2010, he worked as a Postdoctoral Researcher with IIT, Italy. Since October 2009, he has been appointed as a Professor with VUB. In 2013, he received an ERC Starting Grant on new generation compliant actuators. He is currently a Core Lab Manager with Flanders Make. The focus of his research was the use of adaptable compliance of pneumatic artificial muscles in the dynamically balanced biped Lucy. His research interests include cognitive and physical human–robot interaction with core technology using variable impedance actuators with applications in health and manufacturing.